A Low-Cost and Scalable Carbon Coated SiO-Based Anode Material for Lithium-Ion Batteries

Zhihao Huang,[a] Guoju Dang,[b, c] Wenping Jiang,[a] Yuanyu Sun,[a] Meng Yu,[a] Quansheng Zhang,*[a] and Jingying Xie*[b, c]

Silicon monoxide (SiO) is considered as one of the most promising alternative anode materials thanks to its high theoretical capacity, satisfying operating voltage and low cost. However, huge volume change, poor electrical conductivity, and poor cycle performance of SiO dramatically hindered its commercial application. In this work, we report an affordable and simple way for manufacturing carbon-coated SiO—C composites with good electrochemical performance on kilogram scales. Industrial grade SiO was modified by carbon coating using cheap and environment friendly polyvinyl pyrrolidone (PVP) as carbon source. High-resolution transmission electron microscopy (HRTEM) and Raman spectra results show that there is an amorphous carbon coating layer with a thickness of about 40 nm on the surface of SiO. The synthesized SiO—C-650 composite shows great electrochemical performance with a high capacity of 1491 mAh.g^{-1} at 0.1 C rate and outstanding capacity retention of 67.2% after 100 cycles. The material also displays an excellent performance with a capacity of 1100 mAh.g^{-1} at 0.5 C rate. Electrochemical impedance spectroscopy (EIS) results also prove that the carbon coating layer can effectively improve the conductivity of the composite and thus enhance the cycling stability of SiO electrode.

1. Introduction

Lithium-ion battery has been an important energy storage application widely used in portable devices and electric vehicles because of its high energy density and long cycle life.[1–5] To meet the higher capacity requirement of the rapid development of emerging industries such as new energy vehicles and large-scale energy storage stations, it's still necessary to develop higher energy density anode than graphite-based anode.[1,2,6–9] Nowadays, Si-based materials are the most promising material to substitute for graphite-based materials, benefiting from its higher theoretical specific capacity (Si: ~4200 mAhg^{-1}), low working potential (<0.5 V) and abundance in nature.[10–14] Nevertheless, there are two major problem of the Si anode limit its commercial application: the low intrinsic electric conductivity and massive volume change (~300%) during lithiation and delithiation. The severe volume swelling leads to continuous formation of the solid electrolyte interphase (SEI) which cause low cycling efficiency and capacity retention.[5,8,13–16] Silicon monoxide (SiO) was regarded as one of the most promising anode materials substitute for graphite[17–20] thanks to its high theoretical specific capacity (~2400 mAhg^{-1}) and improved cycling stability compared with Si. Li$_2$O and Li$_4$SiO$_4$ were generated during the initial lithiation process,[21–24] could accommodate the volume expansion (~200%) during lithiation-delithiation to a certain extent.[5,25–27] Therefore, SiO is considered to be a more practical material in the transition period from graphite to Si-based anode.[9,15,28] Unfortunately, the formation of inactive Li$_2$O and Li$_4$SiO$_4$ as well as the formation of solid electrolyte interphase (SEI) led to low initial coulombic efficiency (ICE) and poor stability. Volume change, poor electrical conductivity and poor cycle performance of SiO dramatically hindered its commercial application.[16,29–31]

In order to improve the electrochemical properties of SiO materials, one of the most effective strategies is to coat the SiO particle surface with various materials.[32–36] Carbon coated SiO composites were reported to have higher ICE and much better cycle performance than the pristine SiO attributing to the existence of a good electronic conductive carbon coating layer, which can accommodate the volume expansion during cycling and also make isolation from electrolyte and active material thereby leading the formation of favorable SEI film.[21,37–40] As a environmentally friendly and wildly used chemical raw material, polyvinyl pyrrolidone has lower pyrolysis temperature (500 °C), which is beneficial to reduce the cost.[41] Hydrothermal method and sol-gel method can be used for carbon coating at low temperature, which are suitable for solid-liquid and liquid-liquid system, but the process is relatively complex, and the yield is low. Chemical vapor deposition method and pyrolysis method

[a] Z. Huang, W. Jiang, Y. Sun, M. Yu, Prof. Q. Zhang
     Department of Chemical Engineering,
     Shanghai institute of Technology
     Shanghai 201418 (China)
     E-mail: zhangquansheng@sit.edu.cn
[b] G. Dang, Prof. J. Xie
     Department of Research and Development,
     Shanghai Power and Energy Storage Battery System Engineering Technology Research Center
     Shanghai 200245 (China)
     E-mail: xiejingying2007@126.com
[c] G. Dang, Prof. J. Xie
     State Key Laboratory of Space Power-Sources Technology
     Shanghai Institute of space power sources
     Shanghai 200245 (China)

are wildly used for carbon coating on a large scale.[42] Compared with chemical vapor deposition method, pyrolysis method is more convenient and feasible. In this work we synthesized carbon coated SiO by pyrolysis method.

Herein, we report a carbon-coated SiO-based anode material. In this work cheap industrial grade silicon monoxide (SiO) and polyvinyl pyrrolidone (PVP) were used as silicon source and carbon source, respectively. SiO—C composites were synthesized by one-step method through mechanical milling and high temperature pyrolysis processes on kilogram scales. The SiO—C composite with carbon coating layer exhibits high capacity, great cycling stability and a relatively higher initial coulombic efficiency. Our method provides an affordable and simple way for manufacturing SiO—C composites on a large scale.

Figure 1. Schematic illustration of the fabrication process of SiO—C composites.

2. Results and Discussion

The XRD patterns of SiO—C composites heated at different temperatures are shown in Figure 2a. The hump at about $2\theta = 20°-30°$ is corresponding to a typical amorphous phase of Silicon dioxide. The sharp peaks of SiO—C-850 and SiO—C-950 at about 28.4°, 47.3°, and 56.1° are associated with (111) (220) (311) facet respectively, which can be associated to the crystalline phase of Si and the XRD patterns conform to the literature (JCPDS file Card No.27-1402). The crystal diffraction peak of Si in XRD patterns is due to the disproportionation reaction of SiO in the process of pyrolysis above 800 °C.[43,44] Remarkably, there is almost no difference between the XRD pattern of SiO—C-550, SiO—C-650 and SiO—C-750 and pristine SiO, indicating that when the pyrolysis temperature is below 750 °C the amorphous structure of pristine SiO has not been changed during the carbon coating process.[45] Besides, diffraction peaks of graphitic carbon have not been detected from XRD patterns, implying that carbon coating layer generated after pyrolysis process is amorphous nature. Figure 2b shows the Raman spectra of the SiO—C composites synthesized by pyrolysis process. The characteristic peaks located at ~1330 cm^{-1}, 1580 cm^{-1} correspond to the disordered (D) bands and graphene (G) bands of carbon, respectively, and the intensity ratio can be used to describe the degree of graphitization. The results of Raman spectrum show that I_D/I_G ratio is 1.31,1.28,1.26,1.25,1.26 for the SiO—C-550, SiO—C-650, SiO—C-750, SiO—C-850 and SiO—C-950, respectively. The values of I_D/I_G ratio suggest a high degree of disorder within the carbon structure.[46,47] Indicating that the existence of amorphous carbon in composites, which is in accordance with the XRD results.

TGA result of the synthesized SiO—C composites is shown in Figure 3, the carbon content in SiO—C-550, SiO—C-650, SiO—C-750, SiO—C-850 and SiO—C-950 is 7.29%, 4.85%, 4.47%, 3.82% and 3.42%, respectively. With the increase of pyrolysis temperature, the carbon content of the composites decreased gradually.

The microstructure and morphology of pristine SiO and SiO—C composites is shown in Figure 4 by scanning electron microscope(SEM) and high-resolution transmission electron microscope (HRTEM). As shown in Figure 4a and 4b It is not difficult to observe that the prepared SiO—C composites have similar particle size with pristine SiO (Figure 4c and 4d) with an average particle size of 2 μm–4 μm, both samples are composed of irregular particles, indicated that the unique microstructure of SiO was maintained after carbon coating process. Compared with pristine SiO, carbon coating layer makes the surface of SiO particles smoother. The existence of carbon
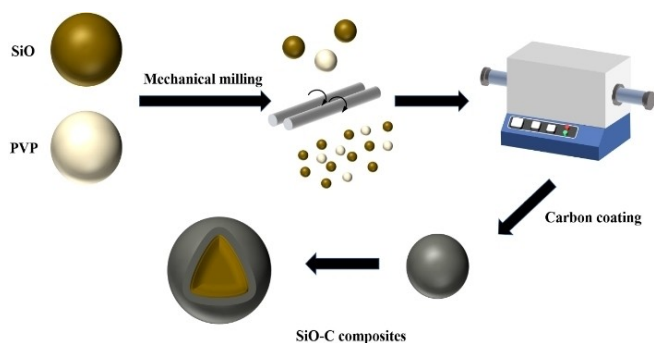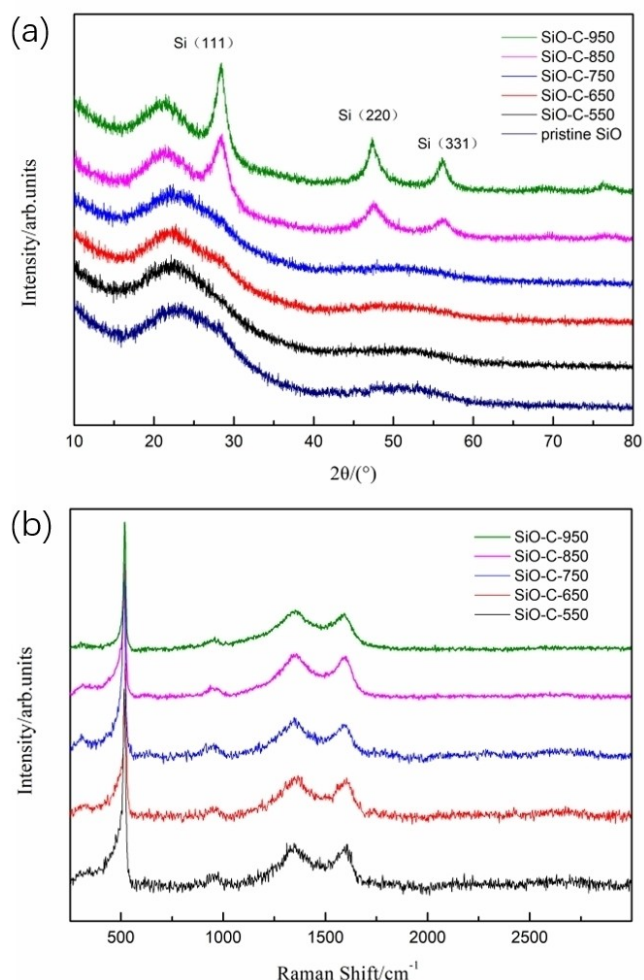

Figure 2. (a) XRD pattern and (b) Raman spectra of the SiO—C samples.

ChemistryOpen

Full Papers
doi.org/10.1002/open.202000341

Chemistry Europe
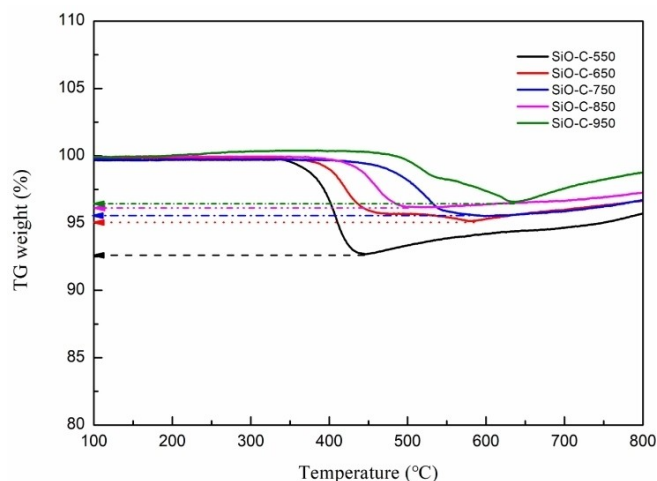European Chemical
Societies Publishing

Figure 3. TGA curves of SiO composites.

coating layer is further confirmed by HRTEM. From Figure 4e–4i, it is not difficult to observe that the surface of SiO–C particles is uniformly coated by a carbon coating layer with about 40 nm thickness. Besides, no lattice fringes belonging to graphite were detected, which proved that the carbon coating layer is amorphous nature, consistent with those of XRD.

In order to evaluate the electrochemical performances of SiO–C composites, galvanostatic charge-discharge test was performed by using a CR 2032-type coin cell. Typical galvanostatic charge-discharge voltage profiles of the SiO–C electrodes at 0.1 C rate between 0.005 and 1.5 V are shown in Figure 5. Significantly, all composites have a long slope voltage plateau between 0.0 V and 0.2 V, which is related to the typical lithiation behaviors of SiO in the initial discharge process.[25] All composites show a relatively stable charging platform from 0.2 to 0.6 V during the delithiation process. SiO–C-550, SiO–C-650, SiO–C-750, SiO–C-850 and SiO–C-850 delivers initial coulombic efficiency of 62.84%, 64.81%, 65.13%, 67.25% and 67.93%,
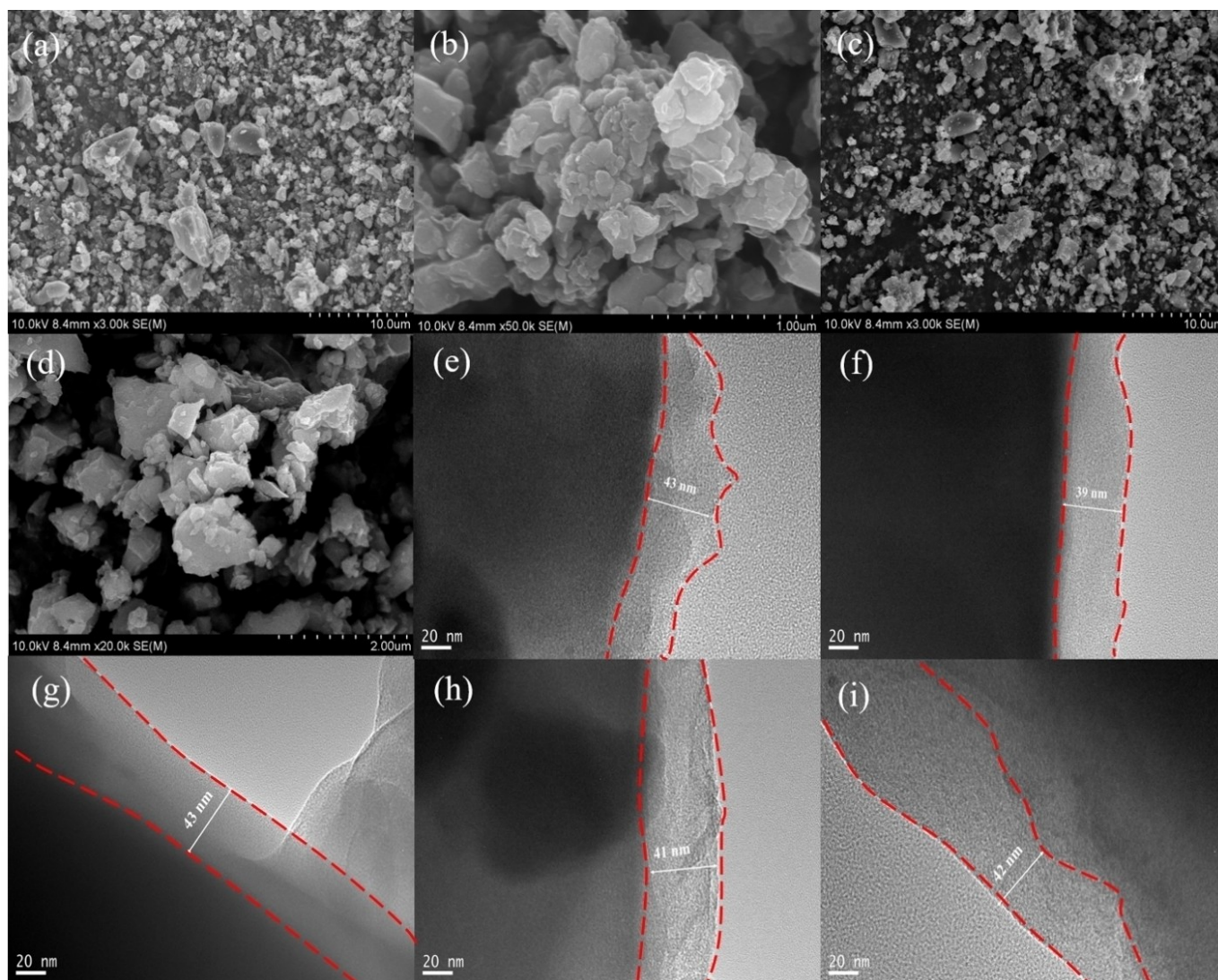

Figure 4. a) and (b) SEM images of pristine SiO ;(c) and (d) SEM images of SiO–C composites ;(e)–(i) HRTEM image of SiO–C-550, SiO–C-650, SiO–C-750, SiO–C-850 and SiO–C-950 composites.
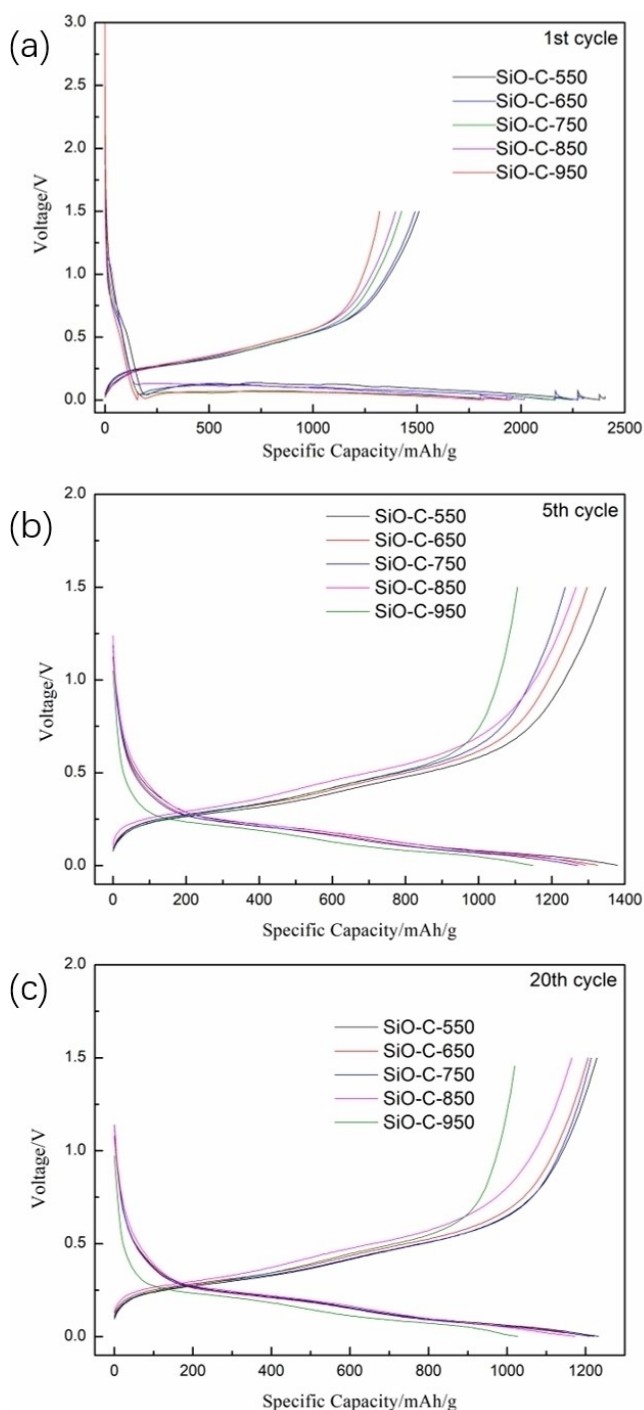
ChemistryOpen

Full Papers
doi.org/10.1002/open.202000341

Chemistry Europe
European Chemical
Societies Publishing

Figure 6. Cycling performance of. SiO–C composites.

1431 mAh.g^{-1}, 1425 mAh.g^{-1}, 1480 mAh.g^{-1} and 1321 mAh.g^{-1} for SiO–C-550, SiO–C-650, SiO–C-750, SiO–C-850 and SiO–C-950 composites, respectively. In terms of cycling performance, the retention of discharge capacity after 100 cycles is 61.6%, 67.1%, 62.6%, 53.1% and 55.9%, respectively (Table 1). After 5 cycles, the coulomb efficiency of all composites reaches almost 100%. With the increase of pyrolysis temperature, the capacity of SiO–C composites decreases slightly, rebounds at 850°C and decreases obviously at 950°C. Comparatively the initial coulombic efficiency of SiO–C composites improves with the increase of pyrolysis temperature. Due to the disproportionation reaction, the initial coulombic efficiency of SiO–C-850 and SiO–C-950 composites are obviously higher, but the capacity retention of these two composites were relatively lower. After 100 cycles, the SiO–C composites still have considerable capacity and retention, which is due to the carbon coating layer. The carbon coating layer greatly improves the conductivity of SiO electrodes. At the same time, the carbon coating provides a buffer layer for the volume expansion stress and protects the integrity of the electrode during lithiation and delithiation. In sharp contrast, the capacity of pristine SiO is almost 0 after 30

Figure 5. (a)–(c) charge-discharge voltage profiles of SiO–C composites for the 1st, 5th and 20th cycles.

respectively. Compared with the discharge-charge voltage profile of SiO–C composites for the 1st cycle, those for the 5th and 20th cycles show that the coulombic efficiency of all composites maintains above 99%, indicating a good reversibility.

The performance of cycle stability and corresponding coulombic efficiency of SiO–C composites are shown in Figure 6a. The initial charge capacities are 1510 mAh.g^{-1},
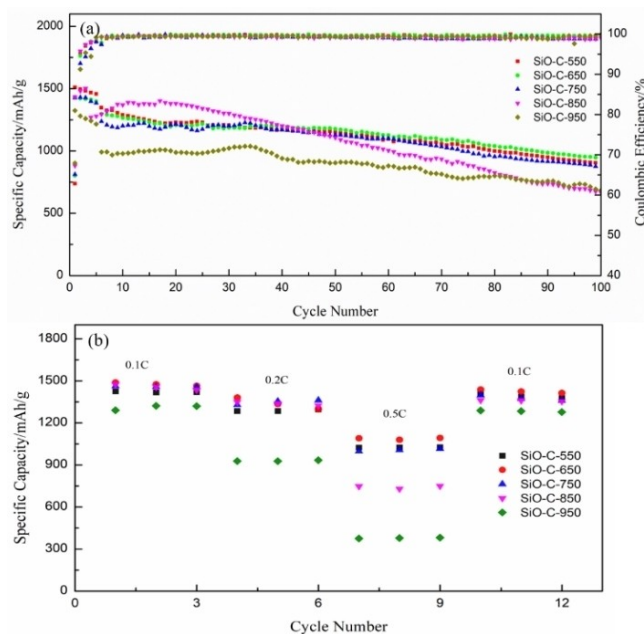
Table 1. The electrochemical performance of SiO–C composites in half cells.

Samples	1st Charge capacity [mAh.g^{-1}]	1st Discharge capacity [mAh.g^{-1}]	ICE [%]	capacity retention [%]
SiO–C-550	1509.9	2402.8	62.84	61.6
SiO–C-650	1491.5	2301.3	64.81	67.2
SiO–C-750	1425.5	2188.7	65.13	62.6
SiO–C-850	1433.4	2131.4	67.25	53.1
SiO–C-950	1321.3	1945.1	67.93	55.9

cycles.[21] In terms of cycling performance and the initial coulombic efficiency, SiO–C-650 exhibited the best.

The rate capability of the SiO–C composite was tested. As plotted in Figure 6b, even at a 0.5 C rate, SiO–C-650 displays an excellent cycling performance with a capacity of 1100 mAh.g^{-1}. Upon C rate returns to 0.1 C, the capacity of the SiO–C-650 electrode can still maintain at1437 mAh.g^{-1}, indicating that it has good electrochemical reversibility and structural integrity even at a high C rate. The great rate capability may attribute to the existence of conductive carbon coating layer, allowing electrons and lithium ions pass through the entire electrode quickly.[48–50]

To further verify the influence of carbon coating layer on conductivity of composites, electrochemical impedance spectroscopy and the equivalent circuit are shown in Figure 7. The Nyquist plots is comprised of a small intercept at high frequency region, a semicircle at the medium frequency region, and an inclined line at the low frequency region, which was corresponding to the ohmic resistance R_s, electrode-electrolyte interface resistance R_{ct}, and the Warburg impedance W, respectively. The corresponding values are listed in Table 2, significantly, SiO–C-650 exhibits the best electrochemical performance, which exhibits the minimum R_{ct} than others. Especially, the R_{ct} value of SiO–C-650 is significantly smaller, implying that carbon coating layer which obtained in 650 °C helps charge transfer easier The EIS fitting result is consistent with the performance of cycle stability of. SiO–C composites that SiO–C-650 exhibited best (82.2 % capacity retention after 50 cycles). These results suggest that carbon coating layer can effectively stabilize the solid-liquid interface between the electrode and electrolyte and improve the conductivity of composites, thus greatly improving the electrochemical performances of SiO–C composites.

The electrochemical performance comparison between our SiO–C-650 anode and previously reported SiO-based anodes was shown in Table 3. Compared with the previously reported SiO-based anodes, SiO–C-650 has high capacity and better cycle performance, and the initial coulombic efficiency needs to be further improved.
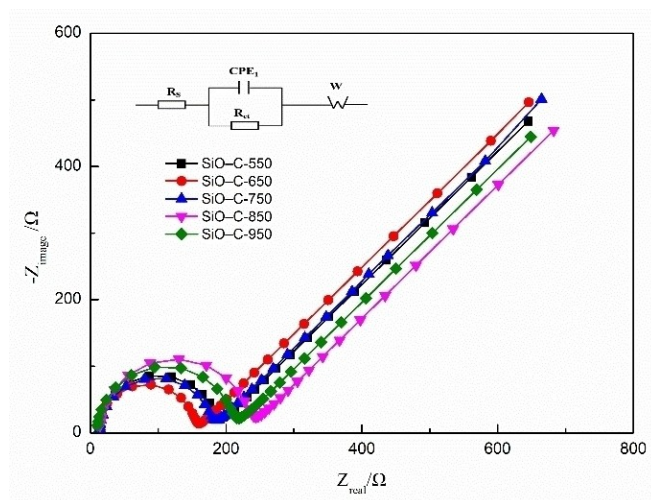
3. Conclusion

In summary, we successfully synthesized the SiO–C composites by mechanical milling and pyrolysis in an affordable and simple way on kilogram scales. For the SiO–C-650 sample, the surface of SiO particles is a carbon coating layer with a thickness of about 40 nm, which can accommodate the volume expansion and increase the conductivity of electrode. As a result, the synthesized SiO–C-650 composite showed great electrochemical performances with a high capacity of 1491 mAh.g^{-1} at 0.1 C rate and an outstanding capacity retention of 67.2 % after 100 cycles. The material also displayed an excellent electrochemical performance with a capacity of 1100 mAh.g^{-1} at 0.5 C rate. Electrochemistry impedance spectroscopy (EIS) results also proved that the carbon coating layer can effectively improve the conductivity of the composite.

Figure 7. The Nyquist plots and corresponding equivalent circuit model of the EIS curves.

Experimental Section

Material preparation

SiO (Taiyuan Hengxin Technology Industry Co., Ltd) and PVP (BASF) as raw materials were ground into micro-sized particles with a mass ratio of SiO:PVP=2:1 through mechanical milling process. The resulted mixture was heated in a tube furnace at 5 °C min^{-1} from room temperature to different temperatures ranging from 550 to

Table 2. EIS fitting result of SiO–C composites.

Samples	$R_s[\Omega]$	$R_{ct}[\Omega]$
SiO–C-550	11.23	166.12
SiO–C-650	11.16	141.94
SiO–C-750	12.12	160.16
SiO–C-850	12.69	215.37
SiO–C-950	11.56	194.4

Table 3. Electrochemical performance comparison between our SiO–C-650 anode and previously reported SiO-based anodes.

Active material	ICE [%]	Capacity [mAh.g^{-1}]	Capacity retention [%]	Ref
SiO$_x$–C	63.1	1200	56.3(100cycles)	[33]
C–SiO–MgSiO$_3$–Si-1100	78.3	1605	60.1(100cycles)	[39]
SiO@C-35	78.6	1151.5	87.2(20cycles)	[43]
SiO–C	77.0	988.3	86.0(100cycles)	[36]
bm–SiO/Ni/rGO	62.4	1021.7	70.5(100cycles)	[44]
SiO–C-650	64.8	1491.5	67.2(100cycles)	This work

950 °C for 2 hours under the Ar_2/H_2 atmosphere, resulting in the carbon-coated composites. PVP was vaporized during pyrolysis and attached to the surface of particles in the form of mist, which is conducive to the formation of a uniform carbon coating layer. The products obtained at the temperature, T, were denoted as SiO−C−T.

Material characterization

Field emission scanning electron microscope (FESEM, Hitachi, S-4800) and high-resolution transmission electron microscopy (HRTEM, JEOL JEM-2100F) was used to investigate the morphology of the samples. The Crystal structure of different samples were investigated by the X-ray diffraction (XRD, Rigaku Ultima IV diffractometer, Cu) in the 2θ range of 10˚-80˚. Raman spectra were obtained by a Raman spectrometer (Thermo Fisher DXRxi) using a 532-nm laser as a light source. A Netzsch STA449F3 Jupiter instrument was used for thermogravimetric analysis (TGA), the test atmosphere is air.

Electrochemical measurements

Electrochemical performance tests were performed with two-electrode CR 2032-type coin cell. The slurries for making electrode were prepared by mixing SiO−C−T, carbon black (Super P) and PAA−Li with a mass ratio of 70:20:10. A homogenously slurry was then coated on copper foil with a loading level of $\sim 1 \, mg/cm^2$, followed by drying 4 h at 80 °C and vacuum drying 10 h at 90 °C. All cells were assembled in an argon-filled glove box (water content <0.1 ppm, oxygen content <0.1 ppm). The electrolyte was 1.2 M $LiPF_6$ in a solvent of ethylene carbonate (EC) and ethylene carbonate (DEC) with a volume ration of 3:7. Commercial lithium foil (750 µm thickness) was used as the counter electrode. The galvanostatic charge-discharge experiments were tested using an LANHE testing system in the potential range of 0.005–1.5 V. Electrochemical impedance spectroscopy (EIS) was analyzed with CHI660E from 100 kHz to 100 mHz.

Conflict of Interest

The authors declare no conflict of interest.

[1] J. W. Choi, D. Aurbach, *Nat. Rev. Mater.* **2016**, *1*, 1–16.
[2] S. Goriparti, E. Miele, F. De Angelis, E. Di Fabrizio, R. P. Zaccaria, C. Capiglia, *J. Power Sources* **2014**, *257*, 421–443.
[3] C. P. Grey, J. M. Tarascon, *Nat. Mater.* **2017**, *16*, 45–56.
[4] M. Li, J. Lu, Z. W. Chen, K. Amine, *Adv. Mater.* **2018**, 30, 1800561.
[5] X. Su, Q. L. Wu, J. C. Li, X. C. Xiao, A. Lott, W. Q. Lu, B. W. Sheldon, J. Wu, *Adv. Energy Mater.* **2014**, *4*, 1300882.
[6] X. B. Cheng, R. Zhang, C. Z. Zhao, Q. Zhang, *Chem. Rev.* **2017**, *117*, 10403–10473.
[7] D. C. Lin, Y. Y. Liu, Y. Cui, *Nat. Nanotechnol.* **2017**, *12*, 194–206.
[8] N. Nitta, F. X. Wu, J. T. Lee, G. Yushin, *Mater. Today* **2015**, *18*, 252–264.
[9] W. Xu, J. L. Wang, F. Ding, X. L. Chen, E. Nasybutin, Y. H. Zhang, J. G. Zhang, *Energy Environ. Sci.* **2014**, *7*, 513–537.
[10] M. Ashuri, Q. R. He, L. L. Shaw, *Nanoscale.* **2016**, *8*, 74–103.
[11] J. B. Chang, X. K. Huang, G. H. Zhou, S. M. Cui, P. B. Hallac, J. W. Jiang, P. T. Hurley, J. H. Chen, *Adv. Mater.* **2014**, *26*, 758–764.
[12] Y. Z. Li, K. Yan, H. W. Lee, Z. D. Lu, N. Liu, Y. Cui, *Nat. Energy* **2016**, *1*, 15029.
[13] B. Liang, Y. P. Liu, Y. H. Xu, *J. Power Sources* **2014**, *267*, 469–490.
[14] Z. D. Lu, N. Liu, H. W. Lee, J. Zhao, W. Y. Li, Y. Z. Li, Y. Cui, *ACS Nano* **2015**, *9*, 2540–2547.
[15] Q. Xu, J. Y. Li, J. K. Sun, Y. X. Yin, L. J. Wan, Y. G. Guo, *Adv. Energy Mater.* **2017**, *7*, 1601481.
[16] X. X. Zuo, J. Zhu, P. Muller-Buschbaum, Y. J. Cheng, *Nano Energy.* **2017**, *31*, 113–143.
[17] F. Dou, L. Y. Shi, P. A. Song, G. R. Chen, J. An, H. J. Liu, D. S. Zhang, *Chem. Eng. J.* **2018**, *338*, 488–495.
[18] J. L. Han, G. R. Chen, T. T. Yan, H. J. Liu, L. Y. Shi, Z. X. An, J. P. Zhang, D. S. Zhang, *Chem. Eng. J.* **2018**, *347*, 273–279.
[19] Y. Jiang, S. Liu, Y. W. Ding, J. L. Jiang, W. R. Li, S. S. Huang, Z. W. Chen, B. Zhao, J. J. Zhang, *J. Power Sources* **2020**, *467*, 228301.
[20] E. Park, J. Kim, D. J. Chung, M. S. Park, H. Kim, J. H. Kim, *ChemSusChem* **2016**, *9*, 2754–2758.
[21] Z. H. Liu, Q. Yu, Y. L. Zhao, R. H. He, M. Xu, S. H. Feng, S. D. Li, L. Zhou, L. Q. Mai, *Chem. Soc. Rev.* **2019**, *48*, 285–309.
[22] M. Miyachi, H. Yamamoto, H. Kawai, T. Ohta, M. Shirakata, *J. Electrochem. Soc.* **2005**, *152*, A2089.
[23] Y. Nagao, H. Sakaguchi, H. Honda, T. Fukunaga, T. Esaka, *J. Electrochem. Soc.* **2004**, *151*, A1572.
[24] Y. Yamada, Y. Iriyama, T. Abe, Z. Ogumi, *J. Electrochem. Soc.* **2010**, *157*, A26.
[25] L. Z. Guo, H. Y. He, Y. R. Ren, C. Wang, M. Q. Li, *Chem. Eng. J.* **2018**, *335*, 32–40.
[26] L. Liu, X. X. Li, G. He, G. Q. Zhang, G. J. Su, C. H. Fang, *J. Alloys Compd.* **2020**, *836*, 155407.
[27] K. Pan, F. Zou, M. Canova, Y. Zhu, J. H. Kim, *J. Power Sources* **2019**, *413*, 20–28.
[28] B. C. Yu, Y. Hwa, J. H. Kim, H. J. Sohn, *Electrochim. Acta* **2014**, *117*, 426–430.
[29] S. Z. Zeng, Y. Niu, J. Z. Zou, X. R. Zeng, H. O. Zhu, J. T. Huang, L. Y. Wang, L. B. Kong, P. G. Han, *J. Power Sources* **2020**, *466*, 228234.
[30] J. Z. Zhang, J. Zhang, T. Z. Bao, X. H. Xie, B. J. Xia, *J. Power Sources* **2017**, *348*, 16–20.
[31] J. Zhao, H. W. Lee, J. Sun, K. Yan, Y. Y. Liu, W. Liu, Z. D. Lu, D. C. Lin, G. M. Zhou, Y. Cui, *Proc. Natl. Acad. Sci. USA* **2016**, *113*, 7408–7413.
[32] X. Y. Dong, X. Zheng, Y. C. Deng, L. F. Wang, H. P. Hong, Z. C. Ju, *J. Mater. Sci.* **2020**, *55*, 13023–13035.
[33] G. W. Hu, K. Z. Zhong, R. H. Yu, Z. H. Liu, Y. Y. Zhang, J. S. Wu, L. Zhou, L. Q. Mai, *J. Mater. Chem. A* **2020**, *8*, 13285–13291.
[34] S. J. Kuang, D. H. Xu, W. Y. Chen, X. Q. Huang, L. Y. Sun, X. Cai, X. Y. Yu, *Appl. Surf. Sci.* **2020**, *521*, 146497.
[35] M. Q. Li, J. W. Gu, X. F. Feng, H. Y. He, C. M. Zeng, *Electrochim. Acta* **2015**, *164*, 163–170.
[36] W. J. Wu, J. Shi, Y. H. Liang, F. Liu, Y. Peng, H. B. Yang, *Phys. Chem. Chem. Phys.* **2015**, *17*, 13451–13456.
[37] C. F. Guo, D. L. Wang, T. F. Liu, J. S. Zhu, X. S. Lang, *J. Mater. Chem. A* **2014**, *2*, 3521–3527.
[38] J. Wang, M. J. Zhou, G. Q. Tan, S. Chen, F. Wu, J. Lu, K. Amine, *Nanoscale.* **2015**, *7*, 8023–8034.
[39] W. J. Wu, Y. H. Liang, H. Y. Ma, Y. Peng, H. B. Yang, *Electrochim. Acta* **2016**, *187*, 473–479.
[40] M. Y. Zhu, Y. B. Shen, L. M. Chang, D. M. Yin, Y. Cheng, L. M. Wang, *Nanoscale.* **2020**, *12*, 13442–13449.
[41] K. M. Koczkur, S. Mourdikoudis, L. Polavarapu, S. E. Skrabalak, *Dalton Trans.* **2015**, *44*, 17883–17905.
[42] T. Chen, J. Wu, Q. L. Zhang, X. Su, *J. Power Sources* **2017**, *363*, 126–144.
[43] M. Mamiya, M. Kikuchi, H. Takei, *J. Cryst. Growth* **2002**, *237–239*, 1909–1914.
[44] M. Mamiya, H. Takei, M. Kikuchi, C. Uyeda, *J. Cryst. Growth* **2001**, *229*, 457–461.
[45] Y. Zhang, G. N. Guo, C. Chen, Y. C. Jiao, T. T. Li, X. Chen, Y. C. Yang, D. Yang, A. G. Dong, *J. Power Sources* **2019**, *426*, 116–123.
[46] Y.-S. Ding, W.-N. Li, S. Iaconetti, X.-F. Shen, J. DiCarlo, F. S. Galasso, S. L. Suib, *Surf. Coat. Technol.* **2006**, *200*, 3041–3048.

[47] C. Kim, S.-H. Park, J.-I. Cho, D.-Y. Lee, T.-J. Park, W.-J. Lee, K.-S. Yang, *J. Raman Spectrosc.* **2004**, *35*, 928–933.

[48] G. Fang, X. L. Deng, J. Z. Zou, X. R. Zeng, *Electrochim. Acta* **2019**, *295*, 498–506.

[49] J. K. Lee, J. H. Lee, B. K. Kim, W. Y. Yoon, *Electrochim. Acta* **2014**, *127*, 1–6.

[50] C. Wang, F. Luo, H. Lu, X. H. Rong, B. N. Liu, G. Chu, Y. Sun, B. G. Quan, J. Y. Zheng, J. J. Li, C. Z. Gu, X. P. Qiu, H. Li, L. Q. Chen, *ACS Appl. Mater. Interfaces* **2017**, *9*, 2806–2814.

[51] H. Lu, J. Y. Wang, B. N. Liu, G. Chu, G. Zhou, F. Luo, J. Y. Zheng, X. Q. Yu, H. Li, *Chinese Physics B.* **2019**, *28*, 068201.

[52] Y. C. Liu, J. Y. Huang, X. Q. Zhang, J. W. Wu, A. Baker, H. Y. Zhang, S. Chang, X. H. Zhang, *J. Alloys Compd.* **2018**, *749*, 236–243.